Article

Peroxide Electroreduction on Bi-Modified Au Surfaces: Vibrational Spectroscopy and Density Functional Calculations

Xiao Li, and Andrew A. Gewirth

J. Am. Chem. Soc., **2003**, 125 (23), 7086-7099• DOI: 10.1021/ja034125q • Publication Date (Web): 14 May 2003

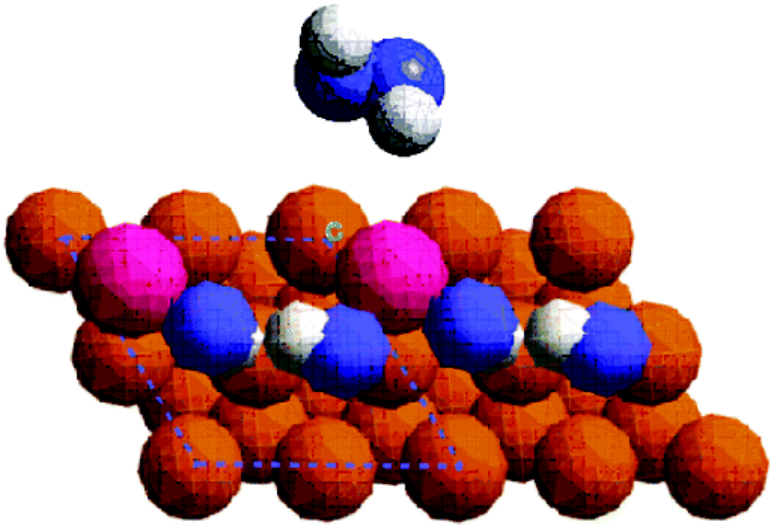

J|A|C|S
ARTICLES
Published on Web 05/14/2003

Peroxide Electroreduction on Bi-Modified Au Surfaces: Vibrational Spectroscopy and Density Functional Calculations

Xiao Li and Andrew A. Gewirth*

Contribution from the Department of Chemistry and Fredrick Seitz Materials Research Laboratory, University of Illinois at Urbana-Champaign, Urbana, Illinois 61801

Received January 11, 2003; E-mail: agewirth@uiuc.edu

Abstract: The mechanism of the electroreduction of peroxide on Bi-submonolayer-modified Au(111) surfaces is examined using surface-enhanced Raman scattering (SERS) measurements along with detailed density functional theory (DFT) calculations. The spectroscopy shows the presence of Bi−OH and Bi−O species at potentials just positive of that where peroxide is reduced. These species are not present in solutions absent either peroxide or Bi. DFT calculations show that peroxide is unstable relative to Bi−OH when Bi is present in the (2 × 2) configuration on Au(111) known from previous work to be catalytically active. The spacing between Bi adatoms is such that peroxide association with two Bi cannot occur without O−O bond cleavage. The full Bi monolayer is catalytically inactive and exhibits none of the Bi−OH or Bi−O signals seen for the active surface. The calculations show that as the Bi coverage becomes greater and the Bi adatom spacing becomes smaller, peroxide can adsorb on Bi without O−O bond rupture. These results indicate an important role for M−OH species in peroxide electroreduction.

1. Introduction

Electroreduction of dioxygen has long been one of the most important reactions in electrochemistry because of its central role in fuel cells, corrosion, and several industrial processes.[1] The complex kinetics of the electroreduction process has been studied for several decades. In acid solution, oxygen reduction proceeds by two pathways depending on electrode composition: a direct four-electron pathway, as shown in eq 1

$$O_2 + 4H^+ + 4e^- \rightarrow 2H_2O \qquad E^0 = 1.229 \text{ V vs NHE} \quad (1)$$

or a peroxide intermediate based two-electron pathway, as shown in eqs 2 and 3.

$$O_2 + 2H^+ + 2e^- \rightarrow H_2O_2 \qquad E^0 = 0.67 \text{ V} \quad (2)$$

$$H_2O_2 + 2H^+ + 2e^- \rightarrow 2H_2O \qquad E^0 = 1.77 \text{ V} \quad (3)$$

For example, on Pt and Ag surfaces, oxygen reduction proceeds by the four-electron pathway, whereas on Au surfaces, the two-electron process dominates and peroxide is produced.[2,3] In both mechanisms, cleavage of the oxygen−oxygen bond seems to be rate-determining. The high dissociation energy of O_2, 494 kJ/mol, leads to slow kinetics and large overpotentials for the four-electron pathway, even on Pt. There are substantial overpotentials to the reduction of peroxide on materials such as Au, even though the O−O bond dissociation energy of H_2O_2, 146 kJ/mol, is considerably less than that of dioxygen. These large overpotentials contribute to lower fuel cell efficiency. There is a clear need to understand the mechanism of O−O bond cleavage in order to develop catalysts with improved kinetics.

Monolayers or sub-monolayers of underpotentially deposited (upd) foreign metal adatoms can act as catalysts for a variety of electrochemical processes.[4] Relevant to oxygen and peroxide reduction, it has long been known that upd Pb,[5] Tl,[6] or Bi[5] can greatly enhance the H_2O_2 reduction rate relative to bare Au(111) and in addition lead to a four-electron reduction mechanism for O_2. However, this enhancement occurs only within a narrow potential range, corresponding to specific structures present on the Au(111) electrode surface.

For Bi upd on Au(111), two different adlattice structures form prior to bulk deposition, but only one is active for H_2O_2 reduction.[7,8] Figure 1 schematically shows the two structures: (a) is a (2 × 2) Bi adlattice with coverage of $\Phi = 25\%$; (b) is the ($p \times \sqrt{3}$) Bi adlattice corresponding to coverage $\Phi = 63-65\%$. As the (2 × 2) Bi structure occurs only in the potential region where the surface is catalytically active for peroxide reduction, this structure is thought to be responsible for the catalytic activity. Recently, surface X-ray scattering (SXS) measurements showed that the (2 × 2) Bi structure remains on

* Author to whom correspondence should be addressed [telephone (217) 333-8329; fax (217) 333-2685; e-mail agewirth@uiuc.edu].

(1) Tarasevich, M. R.; Sadkowski, A.; Yeager, E. *Compr. Treatise Electrochem.* **1983**, *7*, 301−398.
(2) Adzic, R. In *Electrocatalysis*; Lipkowski, J., Ross, P. N., Eds.; Wiley-VCH: New York, 1998; pp 197−242.
(3) Markovic, N. M.; Schmidt, T. J.; Stamenkovic, V.; Ross, P. N. *Fuel Cells* **2001**, *1*, 105−116.
(4) Adzic, R. R.; Tripkovic, A. V.; Markovic, N. M. *J. Electroanal. Chem.* **1980**, *114*, 37−51.
(5) Juettner, K. *Electrochim. Acta* **1984**, *29*, 1597−1604.
(6) Amadelli, R.; Molla, J.; Bindra, P.; Yeager, E. *J. Electrochem. Soc.* **1981**, *128*, 2706−2709.
(7) Niece, B. K.; Gewirth, A. A. *Langmuir* **1996**, *12*, 4909−4913.
(8) Chen, C. H.; Kepler, K. D.; Gewirth, A. A.; Ocko, B. M.; Wang, J. *J. Phys. Chem.* **1993**, *97*, 7290−7294.

10.1021/ja034125q CCC: $25.00

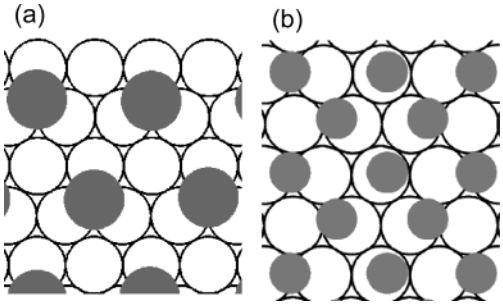

Figure 1. Structures found for Bi upd on Au(111) showing Bi (dark circles) and the Au(111) lattice (open circles): (a) (2 × 2) structure; (b) ($p \times \sqrt{3}$) structure.

the Au surface even during the electroreduction process.[9] However, the mechanism of peroxide electroreduction on this structure and the reason(s) that the full Bi monolayer is inactive are still unknown. The heteronuclear active site afforded by the (2 × 2) Bi adlattice[10] and the inactivity of the full Bi monolayer provide an ideal model system to test ideas about peroxide reduction and compare them with mechanisms proposed for other binuclear systems.[11]

In situ vibrational spectroscopies can provide important information about the interaction of molecules with the immersed electrode surface. Surface infrared spectroscopy is limited by interferences from solution above the electrode surface and by its low sensitivity in the low-frequency region, below 800 cm^{-1}, where metal−oxide and metal−hydroxide modes typically occur.[12] The sensitivity of normal Raman scattering from molecules adsorbed on electrodes is small.[13,14] A tantalizing alternative is presented by surface-enhanced Raman spectroscopy (SERS), which combines requisite surface sensitivity with the ability to obtain information in the low wavenumber region.[15−18] These advantages have a corresponding cost in issues related to the indeterminacy of enhancement mechanism and the requirement of a roughened surface, which can make detailed comparison between structure and spectroscopy problematic. In this study, SERS on roughened polycrystalline Au is used to study the interaction between upd Bi and H_2O_2. Similarities in voltammetry between that from the polycrystalline surface and a well-defined single-crystal electrode allow us to make generalizations concerning the relationship between the spectroscopic signals and the electrode surface structure.

Ab initio calculations have been widely applied to molecule−surface systems over the past few decades.[19] Three different computational methodologies have been utilized to this end: (a) calculations on molecular clusters, (b) the embedded-adsorbate method (EAM), and (c) slab and supercell methods.[20] The properties of the molecule−surface system obtained from cluster calculations are thought to depend strongly on cluster size.[21] The binding energy, geometry, and energetics of step formation on noble metal surfaces (Ag, Au, Pt, etc.) have been studied in detail by using the EAM method.[22] Compared with other methods, supercell calculations are thought to converge more quickly and yield excellent agreement with experiment results.[20] Recently, calculations of this type have examined the interaction between a series of small molecules and metal surfaces.[23] An extensive effort by Norskov and co-workers focuses on d metal adsorption on d metal surfaces.[24]

Relevant to upd, the excess binding energy of noble metal atoms underpotentially deposited on noble metal surfaces has been examined.[25] Huckaby and Blum used thermodynamic considerations to examine upd of Cu on Au(111) with particular emphasis on the phase transition process and structures occurring in the presence of sulfate or bisulfate ions.[26,27] Models based on the density function theory were found to be very useful in understanding the general trend of the lattice constant, binding energy, and underpotential shift of some upd processes.[28] However, the chemisorption of heavy p metal atoms, such as Bi, on Au(111) remains to be examined. A sound understanding of how H_2O_2 associates with the Bi-modified Au surface is crucial to obtaining insight into this catalytic process.

The mechanism of dioxygen reduction on various surfaces in the acid electrochemical environment has been widely studied.[2] On Ag electrodes, electrochemical results show that H_2O_2 reduction is an autocatalytic reaction and the coverage of adsorbed $(OH)_{ad}$ increases with reduction current.[29] On Pt electrodes, both experimental and computational results suggest the presence of an autocatalytic effect arising from surface Pt−OH, which enhances the dissociative adsorption of H_2O_2.[30,31] On Prussian Blue (ferric ferrocyanide) modified Au electrodes, H_2O_2 reduction results in the formation of OH^-.[32] Hydroxide also has been implicated in the Bi upd process and is thought to be weakly adsorbed even in the low-pH region where Bi upd on Au(111) occurs.[7]

In this paper, we use in situ spectroscopy to interrogate the Bi-modified Au surface. In conjunction with detailed ab initio calculations examining the interaction among Bi, H_2O_2, and Au, these measurements provide considerable insight into the mechanism of peroxide electroreduction in this important system.

(9) Tamura, K.; Ocko, B. M.; Wang, J. X.; Adzic, R. R. *J. Phys. Chem. B* **2002**, *106*, 3896−3901.
(10) Chen, C. H.; Gewirth, A. A. *J. Am. Chem. Soc.* **1992**, *114*, 5439−5440.
(11) Solomon, E. I.; Sundaram, U. M.; Machonkin, T. E. *Chem. Rev.* (*Washington, D.C.*) **1996**, *96*, 2563−2605.
(12) Nichols, R. J. In *Adsorption of Molecules at Metal Electrodes*; Lipkowski, J., Ross, P. N., Eds.; VCH: New York, 1992; pp 347−389.
(13) Sobocinski, R. L.; Bryant, M. A.; Pemberton, J. E. *J. Am. Chem. Soc.* **1990**, *112*, 6177−6183.
(14) Shannon, C.; Campion, A. *J. Phys. Chem.* **1988**, *92*, 1385−1387.
(15) Pettinger, B. In *Adsorption of Molecules at Metal Electrodes*; Ross, P. N., Lipkowski, J., Eds.; VCH Publisher: New York, 1992; pp 285−345.
(16) Campion, A.; Kambhampati, P. *Chem. Soc. Rev.* **1998**, *27*, 241−250.
(17) Pemberton, J. E. In *Handbook of Surface Imaging and Visualization*; Hubbard, A. T., Ed.; CRC Press: Boca Raton, FL, 1995; pp 647−666.
(18) Weaver, M. J. *J. Raman Spectrosc.* **2002**, *33*, 309−317.
(19) Over, H.; Tong, S. Y. In *Handbook of Surface Science*; Holloway, S., Richardson, N. V., Eds.; Elsevier: Amsterdam, The Netherlands, 1996; Vol. 1, pp 425−502.
(20) Brivio, G. P.; Trioni, M. I. *Rev. Modern Phys.* **1999**, *71*, 231−265.
(21) Lin, X.; Ramer, N. J.; Rappe, A. M.; Hass, K. C.; Schneider, W. F.; Trout, B. L. *J. Phys. Chem. B* **2001**, *105*, 7739−7747.
(22) Rojas, M. I.; Amilibia, G. E.; Del Popolo, M. G.; Leiva, E. P. M. *Surf. Sci.* **2002**, *499*, L135−L140.
(23) Burch, R.; Daniells, S. T.; Hu, P. *J. Chem. Phys.* **2002**, *117*, 2902−2908.
(24) Ruban, A.; Hammer, B.; Stoltze, P.; Skriver, H. L.; Norskov, J. K. *J. Mol. Catal. A: Chem.* **1997**, *115*, 421−429.
(25) Sanchez, C. G.; Leiva, E. P. M.; Kohanoff, J. *Langmuir* **2001**, *17*, 2219−2227.
(26) Huckaby, D. A.; Blum, L. *J. Electroanal. Chem.* **1991**, *315*, 255−261.
(27) Huckaby, D. A.; Legault, M. D.; Blum, L. *J. Chem. Phys.* **1998**, *109*, 3600−3606.
(28) Leiva, E. *Electrochim. Acta* **1996**, *41*, 2185−2206.
(29) Flatgen, G.; Wasle, S.; Lubke, M.; Eickes, C.; Radhakrishnan, G.; Doblhofer, K.; Ertl, G. *Electrochim. Acta* **1999**, *44*, 4499−4506.
(30) Nakanishi, S.; Mukouyama, Y.; Karasumi, K.; Imanishi, A.; Furuya, N.; Nakato, Y. *J. Phys. Chem. B* **2000**, *104*, 4181−4188.
(31) Anderson, A. B.; Albu, T. V. *J. Electrochem. Soc.* **2000**, *147*, 4229−4238.
(32) Karyakin, A. A.; Karyakina, E. E.; Gorton, L. *Electrochem. Commun.* **1999**, *1*, 78−82.

2. Methodology

All solutions were prepared from ultrapure water (Milli-Q UVplus, Millipore Inc.; 18.2 MΩcm). Reagent grade Bi_2O_3 (Aldrich, 99.999%), H_2O_2 (30%, Fisher), $HClO_4$ (70%, Baker, UltrexII), and H_2SO_4 (Baker, UltrexII) were used for preparing solutions. The working electrode for cyclic voltammetric and rotating disk measurement was a polycrystalline Au disk (Monocrystals Inc.) with a diameter of 1 cm. The crystal was annealed for 3 min in a hydrogen flame and quenched by ultrapure water before experiments.

Cyclic voltammograms were obtained in a glass electrochemical cell using an AFRDE5 (Pine Instrument Co.) potentiostat. The counter electrode was a gold wire (Alfa, 99.9985%, 0.5 mm in diameter), which was flamed every time prior to use. The reference electrode was a Ag/AgCl cell maintained in a separate compartment connected to the cell via a capillary salt bridge to minimize contamination from the reference electrode. All potentials are reported with respect to NHE in this paper. The solutions were deoxygenated by N_2 for 1 h, and an N_2 atmosphere was maintained in the cell during all electrochemical experiments. Rotating disk electrode data were obtained using a Pine model MSRX rotator equipped with a collet to hold the gold crystal.

Before each SERS experiment, the polycrystalline gold was mechanically polished by successively using 9.5, 5.0, 1.0, and 0.3 μm alumina paste on a Buehler Microcloth pad. Between each polishing step the crystal was sonicated for 5 min in ultrapure water. Following polishing, the crystal was roughened electrochemically in 0.1 M KCl.[33,34] The potential was first held at −1.16 V for 10 min and stepped to −0.06 V for 2 min. The potential was then swept from −0.06 to 1.44 V and back for 20 oxidation−reduction cycles at 750 mV/s. During each cycle, the potential was held at −0.06 V for 30 s and then at 1.44 V for 2 s. Finally, the potential was held at −0.36 V for 2 min to desorb adsorbed Cl. After potential cycling, the roughened disk was rinsed with large amounts of ultrapure water.

Room temperature SERS were obtained by using a modification of an in situ cell described previously.[35] A DCM dye laser (Coherent) pumped by the 514.5 nm line of an Ar ion laser (Lexel Laser, 1.5 W) provided the Raman excitation at 668.0 nm. After the beam passed through a laser filter monochromator (Applied Photophysics), the power incident on the Au surface was 20−30 mW. The scattered radiation was collected at 45° relative to the laser excitation by an 85 mm camera lens (Canon) and focused at the entrance slit of a triple monochromator (1877 Triplemate, Spex). A 600 grooves/mm grating dispersed the radiation onto a liquid nitrogen-cooled CCD (Roper Scientific). Spectra were digitally recorded via interface to a computer using WinSpec/32 software (Roper Scientific). The spectrum acquisition time was typically 30 s. Spectra were obtained between 200 and 1600 cm^{-1} at 0.1 V intervals. The system was allowed to equilibrate for 2 min at each potential before spectra were acquired. The spectral resolution was estimated to be 3 cm^{-1}. The baseline for each SERS spectrum was corrected prior to presentation.

Vibrational spectra of some compounds were calculated using the IR/Raman spectrum calculation package within the MSI−Cerius2 program suite.[36] In this program, the forces on the molecule are calculated by a quasi-harmonic approximation, and the second-derivative matrix (Hessian) is used to calculate the vibrational modes. The relative intensity of a mode is calculated from the sum over all atoms of the product of the atomic point charge and its mode displacement vector.

Calculations on periodic structures were carried out using CASTEP[36] in MSI−Cerius2. Density function theory calculations with the generalized gradient approximation (GGA-PW91) were performed.[37] Ultrasoft pseudopotentials were used to describe the electron−core interactions of Au, Bi, O, and H. Valence states include the 5d and 6s shells for Au, 6s and 6p for Bi, 2s and 2p for O, and 1s for H. The electronic wave functions were expanded in a plane wave basis set with an energy cutoff of 400 eV.[38] For total energy calculations a Monkhorst−Pack *k*-point sampling scheme with 12 *k*-points in the supercell was applied. In this work, the Au(111) surface was modeled by a $p(2 \times 2)$ unit cell consisting of three layers and 12 Au atoms. A single Bi adatom on this unit cell mimicked the (2×2) structure observed experimentally.[8] As the slab structure was periodic, higher Bi coverages were achieved by adding one or three more Bi atoms to the $p(2 \times 2)$ Au slab surface, yielding surface coverages of 50 and 100% with respect to the underlying Au, respectively. The vacuum region between slabs was 10 Å. In all cases, surface modifications were applied to only one face of the slab. For Bi adsorption on the Au(111) surface, the topmost gold layer was allowed to relax during the adsorption process, whereas the other atoms were constrained in their position to mimic the bulk crystal. For H_2O_2 adsorption on the Bi/Au(111) surface, only the H_2O_2 was allowed to move; the Bi and Au atoms were fixed in place. Calculations for isolated atoms or molecules were performed in the same supercell arrangement as above. Calculations were performed using an SGI Origin 2000 computer at the National Center for Supercomputing Applications (NCSA).

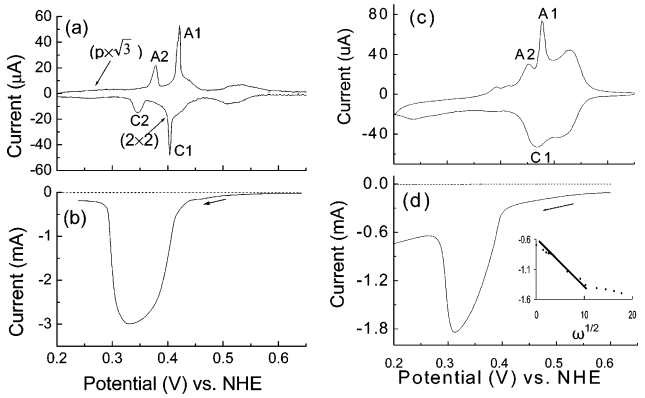

Figure 2. Cyclic voltammogram obtained from (a) Au(111) and (c) Au(poly) in a solution containing 0.5 mM Bi^{3+} + 0.1 M $HClO_4$ (scan rate = 5 mV/s); rotating disk electrode (RDE) voltammogram obtained from (b) Au(111) and (d) Au(poly) in a solution containing 10 mM H_2O_2 + 0.5 mM Bi^{3+} + 0.1 M $HClO_4$ (rotation speed = 400 rpm; scan rate = 5 mV/s). The dashed lines in (b) and (d) show the results of control measurements obtained without Bi^{3+}. The inset in (d) shows a plot of current as a function of the square root of rotation rate obtained at the maximum current. (a) and (b) are adapted from ref 7.

3. Results and Analysis

3.1. Electrochemical Behavior. Cyclic voltammograms of Bi upd on both Au(111) and Au(poly) are shown in Figure 2, panels a and c, respectively. Peaks A and C correspond to the underpotential stripping and deposition peaks of Bi submonolayers on Au surfaces, respectively. As indicated by the arrow in Figure 2a, the Bi(2×2) adlattice forms on Au(111) around 0.4 V.[39] When the potential is moved to more negative values, a denser $(p \times \sqrt{3})$ Bi adlayer forms. The electrochemical behavior of Au(poly) (Figure 2c) also exhibits features due to the upd of Bi. Relative to the voltammetry obtained from the single crystal, the peaks from Au(poly) are broader[40,41] and are

(33) Stolberg, L.; Lipkowski, J.; Irish, D. E. *J. Electroanal. Chem.* **1991**, *300*, 563−584.
(34) Gao, P.; Gosztola, D.; Leung, L.-w. H.; Weaver, M. J. *J. Electroanal. Chem.* **1987**, *233*, 211−222.
(35) Biggin, M. E.; Gewirth, A. A. *J. Electrochem. Soc.* **2001**, *148*, C339−C347.
(36) Cerius^2 software release 4.8, 2002; Molecular Simulations, Inc.; San Diego, CA.
(37) Bilic, A.; Reimers, J. R.; Hush, N. S.; Hafner, J. *J. Chem. Phys.* **2002**, *116*, 8981−8987.
(38) Yourdshahyan, Y.; Zhang, H. K.; Rappe, A. M. *Phys. Rev. B* **2001**, *63*, 1405.
(39) Oh, I.; Biggin, M. E.; Gewirth, A. A. *Langmuir* **2000**, *16*, 1397−1406.

shifted some 0.05 V to more positive potentials. This behavior is consistent with that reported by Jüttner.[42] The shift in energy between the single crystal and polycrystalline systems likely relates to the much higher density of steps on the latter surface. It is well understood that the Gibbs energy of adsorption on a step is higher than that on a terrace.[43] This higher energy makes the upd on stepped and open surfaces occur at more positive potentials relative to the (111) face.

Panels b and d of Figure 2 show the RDE i-E response in cathodic scans from Au(111) and Au(poly) in a solution containing 0.5 mM Bi^{3+} + 10 mM H_2O_2 + 0.1 M $HClO_4$ obtained at a rotation rate of 400 rpm and a scan rate of 5 mV/s. At positive potentials ($E > 0.5$ V), the current is nearly zero. Scanning negatively to below 0.5 V, the cathodic current begins to flow. Around 0.4 V, the current associated with the electroreduction of H_2O_2 rises abruptly; this is catalyzed by a Bi (2×2) adlayer. In Figure 2b,d, the dashed lines show the response from solutions absent Bi. No cathodic current was observed for either system, indicating the importance of Bi for the electroreduction activity. At 0.33 V, the current on both surfaces reaches maximum and begins to drop abruptly upon further negative scanning. This drop is associated with the transformation of the Bi adlayer from the (2×2) to ($p \times \sqrt{3}$) structures on Au (111).[39] The RDE i-E responses from both Au(111) and Au(poly) are remarkably similar both in magnitude of current and in potential limits of the window of electroreduction activity. Residual electroreduction activity on the Au(poly) surface at negative potentials may be associated with the H_2O_2 reduction by the denser Bi adlayer on the polycrystalline Au surface.

The inset to Figure 2d shows the magnitude of the maximum current as a function of rotation speed as the speed is varied from 0 to 4000 rpm. The current increases linearly with the square root of the angular velocity of the disk when the rotation rate is <1000 rpm. This relationship resembles the characteristic curve for a totally mass transfer limited reaction at an RDE described by the Levich equation.[44] As the rotation speed increases, the current saturates, because the surface reaction becomes rate-limiting. A similar saturation speed was reported for the Au(111) case.[39]

3.2. SER Spectra. SERS is used to investigate species on the surface during the electrocatalytic event. Shown in Figure 3 are SER spectra of electrochemically roughened Au immersed in (a) 0.1 M $HClO_4$, (b) 10 mM H_2O_2 + 0.1 M $HClO_4$, and (c) 0.5 mM Bi^{3+} + 0.1 M $HClO_4$ solutions. To the left of each potential scale is the anodic scan, whereas on the right is the cathodic scan. Only that part of the spectrum exhibiting features is shown.

3.2.1. SERS from Au(poly) with Perchlorate Alone. In 0.1 M $HClO_4$, three peaks labeled 2, 3, and 5 are visible, as indicated by arrows in Figure 3a. Peak 5 at 937 cm^{-1} is well understood to be the symmetric stretching mode of the perchlorate ion $\nu(ClO_4^-)$.[45] The intensity of peak 5 increases as the potential moves to positive values and decreases when the potential is returned negatively. This behavior is attributed to the adsorption of perchloric ion on the gold surface,[46] which is enhanced at positive potentials.

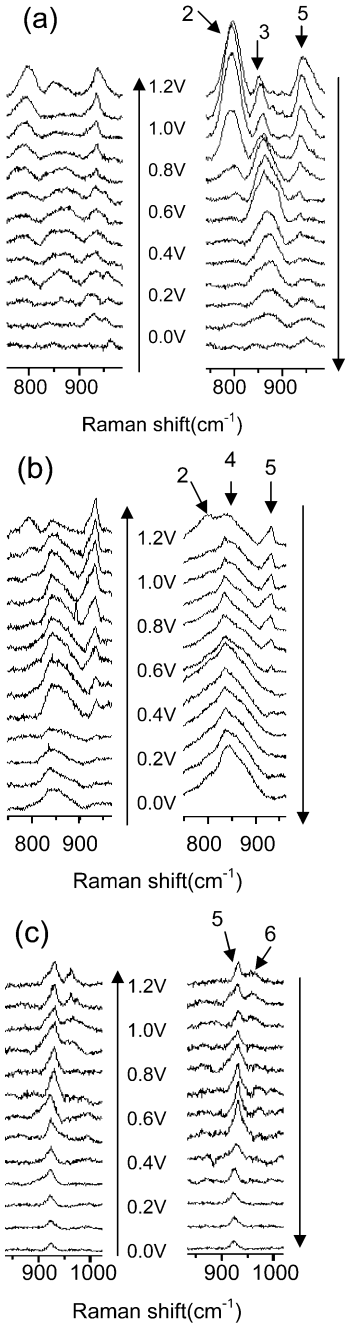

Figure 3. SER spectra from Au(poly) in (a) 0.1 M $HClO_4$, (b) 10 mM H_2O_2 + 0.1 M $HClO_4$, and (c) 0.5 mM Bi^{3+} + 0.1 M $HClO_4$. The anodic potential sweep from 0 to 1.2 V is shown on the left of each panel, whereas the cathodic sweep is shown on the right.

Peak 3 at 850 cm^{-1} is assigned to the twisting mode of H_2O in the clathrate structure formed by the perchlorate above the Au surface, as has been discussed previously.[47,48] There has long

(40) Vaskevich, A.; Rubinstein, I. *J. Electroanal. Chem.* **2000**, *491*, 87−94.
(41) Schmidt, V. M.; Stumper, J.; Schmidberger, J.; Pastor, E.; Hamelin, A. *Surf. Sci.* **1995**, *335*, 197−203.
(42) Sayed, S. M.; Juettner, K. *Electrochim. Acta* **1983**, *28*, 1635−1641.
(43) Hamelin, A.; Lipkowski, J. *J. Electroanal. Chem. Interfacial Electrochem.* **1984**, *171*, 317−330.
(44) Bard, A. J.; Faulkner, L. R. *Electrochemical Methods*: *Fundamentals and Applications*; Wiley: New York, 1980.
(45) Ratcliffe, C. I.; Irish, D. E. *Can. J. Chem.* **1984**, *62*, 1134−1144.
(46) Ataka, K.; Yotsuyanagi, T.; Osawa, M. *J. Phys. Chem.* **1996**, *100*, 10664−10672.
(47) Karelin, A. I. *Zh. Strukt. Khim.* **1991**, *32*, 51−61.
(48) Beden, B.; Melendres, C. A.; Bowmaker, G. A.; Liu, C.; Maroni, V. A. In *Sychrotron Techniques in Interfacial Electrochemistry*; Melendres, C. A., Tadjeddine, A., Eds.; Kluwer: Dordrecht, The Netherlands, 1994; Vol. 432, pp 433−449.

been an understanding that $HClO_4$ forms a $HClO_4 \cdot 5.5H_2O$ clathrate(I)[49] at the interface with the ClO_4^-, probably in both the (5^{12}) and ($5^{12}6^2$) voids of the host structure. At room temperature, this structure decays rapidly perpendicularly to the surface.

Peak 2 at 790 cm^{-1} belongs to the bending vibration of $OH_{ads}^{\gamma-}$, which is strongly adsorbed on the Au surface.[50,51] This band appears only at high potentials ($E > 0.7$ V), and its intensity increases as the potential increases. The adsorption of OH^- on Au is known to occur as the potential nears the Au oxidation region.[52]

3.2.2. SERS with Added H_2O_2. Figure 3b shows a SER spectrum obtained from a Au surface immersed in 0.1 M $HClO_4$ and 10 mM H_2O_2. The spectrum exhibits three peaks, labeled 2, 4, and 5. Peaks 2 and 5 are assigned to the $\delta(OH_{ads}^{\gamma-})$ and $\nu(ClO_4^-)$ modes, respectively, because the energy and potential-dependent behaviors of these bands are identical with the peroxide-free case. However, peak 3, at 850 cm^{-1} associated with the twisting mode of H_2O in the perchlorate clathrate, is not observed. The disappearance of this band may be due to the collapse of the clathrate structure near the Au surface due to the addition of peroxide.

Figure 3b shows a new peak at 840 cm^{-1}, labeled peak 4. This is the characteristic O−O stretch of H_2O_2. Over the potential range studied in these measurements, the magnitude and energy of this band change little, indicating that little interaction between H_2O_2 and Au occurs. The voltammetry also indicates that no H_2O_2 reduction occurs in this potential range. Although peak 4 is ostensibly close in energy to the 850 cm^{-1} band assigned to peak 3 [associated with $\tau(H_2O)$], the presence of peak 4 throughout the potential range examined stands in contrast to peak 3, which disappears at negative potentials. The different potential dependences of peaks 3 and 4, along with their small but measurable energy difference, serve to distinguish the two peaks from each other.

3.2.3. SERS with Added Bi^{3+} . Figure 3c shows the SER spectra of the roughened Au (poly) in the presence of 0.5 mM Bi^{3+} under potential control. Only two peaks, peaks 5 and 6, are present throughout the potential range studied. Peak 5 is associated with $\nu(ClO_4^-)$ as before and is minimized at negative potentials.

The new peak, 6, at 963 cm^{-1}, appears only at high potentials ($E > 0.9$ V). It is assigned to the bending mode of bismuth dihydroxide $\delta_s[Bi(OH)_2]$, which will be discussed later in detail.

3.2.4. SERS with both Bi and H_2O_2. Figure 4 shows the SER spectra obtained from a Au(poly) surface in a solution containing 0.5 mM Bi^{3+} + 10 mM H_2O_2 + 0.1 M $HClO_4$. Three features are observed in the low-energy region at 625 cm^{-1} (peak 1), 936 cm^{-1} (peak 5), and 972 cm^{-1} (peak 6).

Peak 5 at 936 cm^{-1} is assigned to the $\nu(ClO_4^-)$ stretch, and its intensity increases as the potential increases, which is the same behavior observed in blank solution. Alternatively, we did not observe the band associated with peak 4, the ν(O−O) stretch for H_2O_2 at 840 cm^{-1}, which was observed from H_2O_2-containing solutions absent Bi. This indicates that H_2O_2 is not present as a stable species at the surface with the addition of Bi. Peaks 2 and 3 are not observed for what is likely the same reasons they were absent in the spectra from Bi-containing solutions shown in Figure 3c.

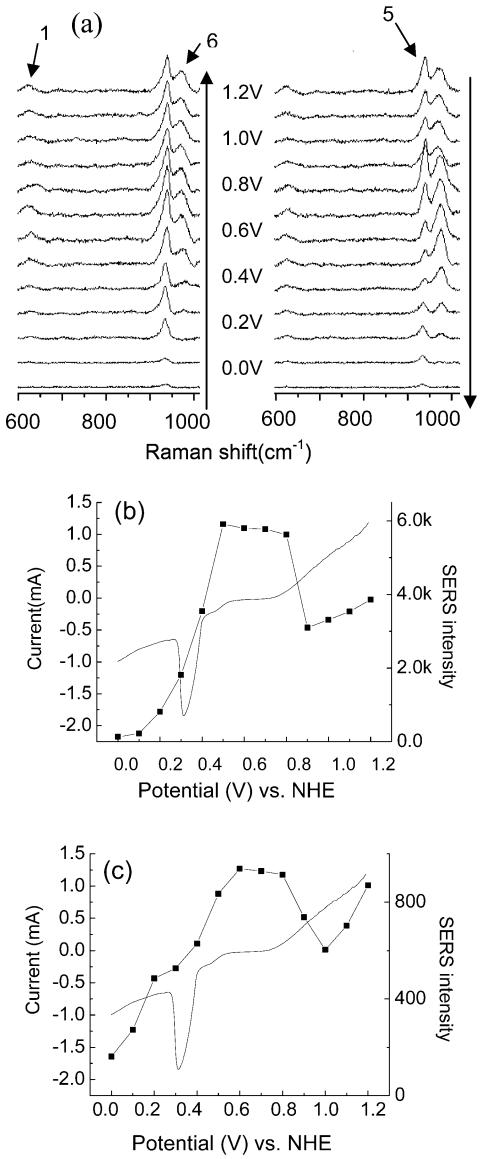

Figure 4. (a) SER spectra from Au(poly) immersed in a solution containing 0.5 mM Bi^{3+} + 10 mM H_2O_2 + 0.1 M $HClO_4$. The anodic potential sweep from 0 to 1.2 V is shown on the left, and the cathodic sweep is on the right. (b, c) Potential dependence of SER spectra intensity (●) from (b) peak 6 δ_s [Bi(O−H)$_2$] and (c) peak 1 $\nu(Bi_2O_2)$ overlayed with the cathodic RDE scan at 5 mV/s obtained in the same solution (solid line).

Two additional peaks (1 and 6) at 625 and 972 cm^{-1}, respectively, are also observed. We now address possible assignments for these peaks. First, they could be associated with gold oxide species. However, it is now clear that gold oxide has SER active peaks only in the spectral region between 400 and 600 cm^{-1}.[53] The gold oxide mode is assigned to a band around 570 cm^{-1} and gold hydroxide to a band around 580 cm^{-1}. In addition, we do not observe peaks 1 and 6 in solutions absent Bi. Second, these peaks could be associated with perchlorate. However, these peaks are not observed in pure

(49) Borkowska, Z.; Cappadonia, M.; Stimming, U. *Electrochim. Acta* **1992**, *37*, 565−808.
(50) Zou, S.; Chan, H. Y. H.; Williams, C. T.; Weaver, M. J. *Langmuir* **2000**, *16*, 754−763.
(51) Savinova, E. R.; Zemlyanov, D.; Pettinger, B.; Scheybal, A.; Schlogl, R.; Doblhofer, K. *Electrochim. Acta* **2000**, *46*, 175−183.
(52) Hamelin, A. *J. Electroanal. Chem.* **1996**, *407*, 1−11.
(53) Desilvestro, J.; Weaver, M. J. *J. Electroanal. Chem. Interfacial Electrochem.* **1986**, *209*, 377−386.

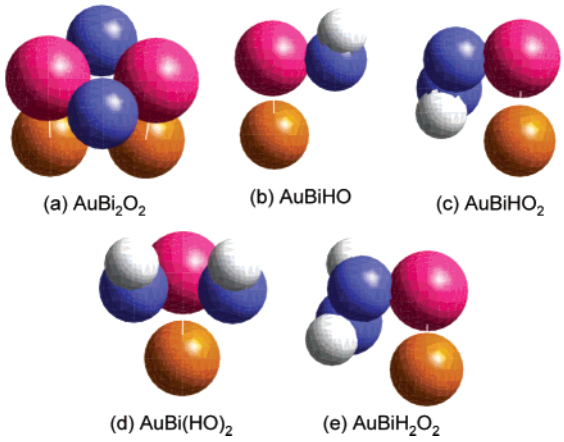

Figure 5. Geometry of compounds from O, H, and Bi atoms from which vibrational frequencies were calculated. Au, Bi, O, and H atoms are orange, pink, blue, and white balls, respectively.

perchlorate solution at any potential. We conclude that peaks 1 and 6 are associated with Bi species present on the surface.

We now examine possible Bi compounds that might be present on the Au surface. $Bi(ClO_4)_3$ exhibits features around 937 and 1054 cm^{-1},[54] but has no peak around 970 cm^{-1}. We thus look to a BiO species, especially because previous work strongly suggested that OH^- functions as the co-adsorbed anion in the (2 × 2) Bi system.[7] Possible BiO-containing species considered included BiOH, BiO, O−Bi−O, $Bi(O_2)$, and Bi_2O_2. Among possible Bi−O assignments, the asymmetric stretch from the Bi_2O_2 four-atom tetracycle is found to occur at 645 cm^{-1}.[55] There are no other BiO-related modes in these species within at least 125 cm^{-1} of the 625 cm^{-1} band we observed. We thus tentatively relate the 625 cm^{-1} feature to this species.

To clarify the assignment made above and to provide insight into the assignment for bands 1 and 6, we performed calculations of possible Bi−O vibrational modes. Shown in Figure 5 are several possible bismuth peroxide and hydroxide compounds. For simplicity, all Bi atoms are associated with only one Au atom to simulate the Au surface. The tetracycle Bi_2O_2, bismuth hydroxide, bismuth hydroperoxo, bismuth dihydroxide, and bismuth hydrogen peroxide are shown in (a), (b), (c), (d), and (e), respectively.

The calculated vibrational modes from these models are listed in Table 1. Interestingly, two vibrational modes match the experiment results. First, the (O−H) bending mode from bismuth dihydroxide is calculated to occur at 979 cm^{-1} as a fairly intense band. This energy is very close to our peak 6 at 972 cm^{-1}. Second, the asymmetric stretch mode of (Bi−O) in the Bi_2O_2 tetracycle is calculated to occur as an intense peak at 639 cm^{-1}, which agrees well with the 645 cm^{-1} mode observed by Malt'sev.[55] There are no other intense bands at energies near the experimental values for peaks 1 and 6 obtained in any of the calculations on these model species.

The energy and assignments of all the bands observed in the SERS measurements are given in Table 2. Finally, we repeated the SERS measurements using 0.1 M H_2SO_4 rather than $HClO_4$ as the supporting electrolyte. Although minor intensity differences in bands were noted, there are no differences in energy

Table 1. Results of Vibrational Frequency Calculations for Bi−OH and Bi−O Compounds[a]

	$Au_2Bi_2O_2$	AuBiOH	$AuBiO_2H$	$AuBi(OH)_2$	$AuBiH_2O_2$
ρ(Au−Bi)	65 vw		57 vw		
ν(Au−Bi)	149 vw	140 vw	155 vw	139 vw	126 vw
ν_s(Bi−O)	161 vw	538 vw	652 vw	164 vw	642 vw
ν_{as}(Bi−O)	639 vs			532 vw	
ω(Bi−O)	271 s			175 vw	311 w
ρ(Bi−O)	564 s			529 vw	
δ(Bi−O)	615 vw		110 vw	264 vw	892 m
τ(Bi−O)		168 vw			
τ(O−H)		125 s	245 s	224 m	289 m
ω(O−H)				358 m	
ρ(O−H)				942 m	1838 vs
δ(O−H)		1039 vs	1883 s	979 s	2012 vw
ν_{as}(O−H)		3733 s	3734 vs	3611 m	3720 m
ν_s(O−H)				3616 s	3769 s
ν(O−O)			1460 w		1486 vw

[a] vs, relative IR intensity = 1; s, relative IR intensity between 0.7 and 0.99; m, relative IR intensity between 0.3 and 0.7; w, relative IR intensity between 0.1 and 0.3; vw, relative IR intensity between 0 and 0.1

Table 2. SER Peak Assignment from Different Solutions[a]

	$\nu_{as}(Bi_2O_2)$	$\delta(OH_{ads}{}^{\gamma-})$	$\tau(H_2O)$	ν(O–O)	$\nu_s(ClO_4{}^-)$	$\delta_s(Bi(O–H)_2)$
peak label	1	2	3	4	5	6
0.1 M $HClO_4$		790	850		937	
0.5 mMBi^{3+} 0.1 M $HClO_4$					935	963
10 mMH_2O_2 0.1 M $HClO_4$		791		840	935	
0.5 mMBi^{3+} 10 mMH_2O_2 0.1 M $HClO_4$	625				936	972

[a] Energies are in cm^{-1}.

or behavior of bands upon addition of the various constituents described above. This suggests that the electrolyte does not play a role in the catalysis.

3.2.5. Potential-Dependent Behavior of Bands 1 and 6. Figure 3c shows that peak 6 appears in the Bi-containing solution without peroxide only at high potential. The appearance of peak 6 in this solution appears to be coincident with the potential where the one-electron oxidation of Au to form AuOH occurs. The presence of the AuOH species may precipitate the formation of BiOH compounds, as well.

Panels b and c of Figure 4 show SERS intensities for peaks 6 and 1 as a function of potential superimposed on the cathodic current associated with H_2O_2 electroreduction. Peak 1 [ν_{as}-(Bi_2O_2)] achieves maximum intensity at 0.6 V, whereas peak 6 [δ_s(Bi(O−H)$_2$)] reaches maximum at 0.5 V during the cathodic scan. As in the case where peroxide is absent, peak 6 grows in again at high potentials ($E \approx 1.2$ V), coincident with Au oxidation.[56] The intensity of both modes decreases as the potential is scanned cathodically from potentials where Au oxidation occurs. After a local minimum, the intensity of peaks 1 and 6 rises as the potential moves to more negative values and reaches maximum at 0.5−0.6 V. At more negative potentials, the lower intensity for both peaks is correlated with the formation of the denser full Bi adlayer. Interestingly, the maximum intensity for both peaks 1 and 6 occurs at potentials ~0.1−0.2 V more positive than the maximum in peroxide

(54) Chumaevskii, N. A.; Ivanova, T. A.; Tarasov, V. P. *Zh. Neorg. Khim.* **1992**, *37*, 2064−2070.
(55) Konnov, S. A.; Serebrennikov, L. V.; Mal'tsev, A. A. *Zh. Fiz. Khim.* **1981**, *55*, 2893−2896.
(56) Angerstein-Kozlowska, H.; Conway, B. E.; Hamelin, A.; Stoicoviciu, L. *J. Electroanal. Chem.* **1987**, *228*, 429−453.

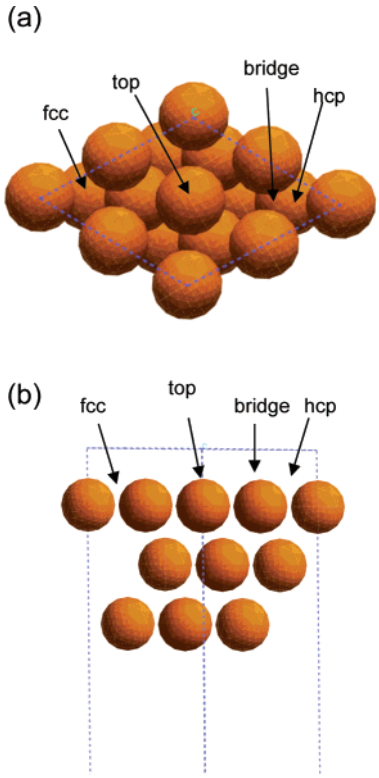

Figure 6. Geometry of the (2 × 2) Au(111) slab used in these calculations. The slab contains three layers and 12 Au atoms (orange balls). Top and side views are shown in (a) and (b), respectively.

Table 3. Comparison of Calculated and Experimental Values for the Au(111) Surface

	calcd	exptl
a_0 (Å)	4.03	4.08
γ (erg/cm^2)	1188	1045−1410

electroreduction current on the Au(poly) surface. The presence of a hydroxide species on the Bi/Au(111) surface in the potential region coincident with the appearance of the (2 × 2) adlattice was inferred from chronocoulometric measurements.[7]

3.3. Calculation Results. The SERS results presented above strongly support a role for Bi−OH species in the electrocatalytic reduction of peroxide to water. Intriguingly, the presence of a feature at 625 cm^{-1} in the SERS is associated with an in-plane Bi_2O_2 tetracycle. To evaluate this and other aspects of the Bi active site, we performed density functional calculations to examine the interplay of the various species on the Au surface during electrocatalysis.

3.3.1. Calculation for Bare Au(111). As a first test of the accuracy of our calculations, we computed the bulk and surface structural properties of Au(111). Figure 6 schematically shows the geometry of the Au(111) surface. The top view and the side view of the slab are shown in (a) and (b), respectively. The blue line outlines the (2 × 2) unit cell. The calculation optimized the geometry of this system by minimizing the total energy. Table 3 shows a comparison of the properties of this surface calculated from our model with the results of experiment. The calculated value of the lattice constant, $a_0 = 4.03$ Å, matches well with the corresponding experimental value $a_0 = 4.08$ Å. The calculated surface energy, $\gamma = 1188$ erg/cm^2, is within the range of reported experimental values, $\gamma = 1045-1410$ erg/cm^2.[57]

Table 4. Comparison of Results for Bi Adsorption on Au(111) in Different Sites

	bridge[e]	top[e]	hcp (relaxed)[f]	fcc (relaxed)[f]
$-E_{ad}$[a] (eV)	4.139	3.034	4.537	4.544
$\Delta z_{(Bi-Au1)}$[b] (Å)	2.16	2.31	2.08	2.10
q_{Au}[c] (e)	−0.32	−0.67	−0.31	−0.30
q_{Bi}[c] (e)	0.78	0.78	0.83	0.81
d(Au−Bi)[d] (Å)	2.6770	2.6870	2.6850	2.6767

[a] Adsorption energy E_{ad}, calculated as the difference between E_{Bi} (the free Bi atom energy), $E_{Au(111)}$ [the isolated Au(111) slab energy], and E_{AuBi} (the Bi adsorption on the slab energy). [b] Vertical distance between Bi and the Au surface. [c] Calculated Mulliken charge population of the Bi atom or the Au atom that is closest to the Bi atom. [d] Distance between the Bi atom and the nearest Au atom. [e] The whole slab is constrained during the calculation. [f] The top layer and Bi atom are relaxed while the lower two layers are constrained.

3.3.2. Calculation for Bi/Au(111) (25% Coverage). Figure 6 shows four possible adsorption sites for a single Bi atom on Au(111). These sites—on top, bridge, 3-fold fcc, and 3-fold hcp—were all examined as possible sites for Bi adsorption.

The adsorption energy and spacing for a single Bi atom on the Au(111) surface in the four possible adsorption sites is shown in Table 4. Geometry optimization always leads to placement of the Bi adatom in either the 3-fold fcc or 3-fold hcp site, indicating that bridge and on-top adsorptions are unstable relative to these two sites. To calculate the adsorption energy for the on-top or bridge site, we fixed the position of both the Bi adatom and the Au surface during calculation. Moving the Bi atom closer to or further from the surface allows several energies to be calculated. The results given in Table 4 are the lowest energy case for these two sites. In case of adsorption on fcc and hcp sites, both the Bi atom and the first layer of surface are relaxed.

Table 4 shows that 3-fold fcc or 3-fold hcp adsorption is favored relative to the other two possibilities. In the hcp site, the Bi adatom has the highest charge: 0.83 e. Adsorption on the fcc site is slightly stabilized relative to hcp by 0.007 eV, and the Bi adatom is almost 0.01 Å closer to Au in the fcc case relative to hcp. These small numbers do not allow a clear distinction to be made between the two sites on the basis of the calculation. Adsorption of Bi into both hcp and fcc 3-fold sites was inferred from preliminary X-ray scattering results on the Bi/Au(111) system.[58] In what follows, only Bi adsorption into the fcc 3-fold hollow site is considered.

Figure 7 shows the calculated Mulliken population charge for the atoms in the 25% Bi fcc adsorption on Au(111) configuration. The Mulliken population charge calculation has been shown to be a good method to simulate experimental results.[59,60] In the figure, the Bi atom is removed to a position above the surface in order to show all of the Au atoms. Compared with the bare Au(111) surface, the calculated charge on the Au atoms in the second and third layers changes little (±0.06 e). On the other hand, the charge on the Au atoms in the first layer changes much more. For Au atoms directly in contact with the Bi adatom, the calculated charge increases from −0.06 e to between −0.26 and −0.30 e. Interestingly, the charge on the Au atom in the center of the unit cell in the first layer,

(57) Cosandey, F.; Madey, T. E. *Surf. Rev. Lett.* **2001**, *8*, 73−93.
(58) Oh, I.; Gewirth, A. A.; Robinson, I. K. 2003, manuscript in preparation.
(59) Ellis, D. E.; Guenzburger, D. *Adv. Quantum Chem.* **1999**, *34*, 51−141.
(60) Gross, K. C.; Seybold, P. G.; Hadad, C. M. *Int. J. Quantum Chem.* **2002**, *90*, 445−458.

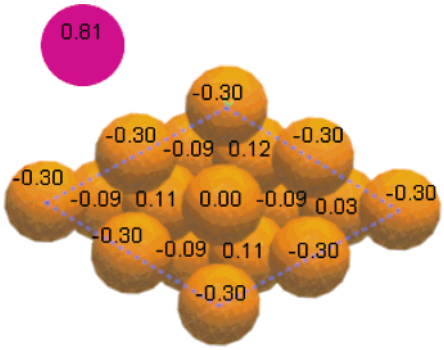

Figure 7. Schematic showing calculated Mulliken charges following adsorption of one Bi at the fcc site of the Au(111) surface. For clarity, the Bi atom (pink ball) is placed above the surface in this figure.

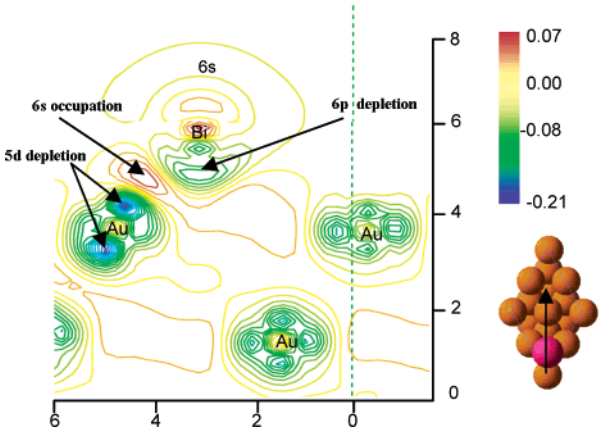

Figure 8. Charge density difference plot for a single Bi adatom adsorbed on the fcc site of Au(111). The plane of the plot is normal to the Au surface and contains the arrow shown in the lower right corner of the figure, where the Bi adatom is represented in pink. The unit of charge density is e/Å^3. The unit of both axes is Å.

which is not in direct contact with the Bi, is calculated to be 0 e. This result suggests that this Au is somewhat more positive than the other Au atoms on the surface. Indeed, this Au is postulated to be the site of interaction with poisons, such as SCN^-, as discussed in previous work.[39]

To understand the interaction between the Bi adatom and the Au surface, the total charge density difference, $\Delta\rho(r)$, for Bi/Au(111) was calculated as

$$\Delta\rho(r) = \rho_{Bi/Au(111)}(r) - \rho_{Bi}(r) - \rho_{Au(111)}(r) \qquad (4)$$

where $\rho_{Bi/Au(111)}(r)$, $\rho_{Bi}(r)$, and $\rho_{Au(111)}(r)$ are the total charge density distribution of the Bi/Au(111) system, free Bi atom, and isolated Au (111) slab, respectively. These charge densities are superimposed with each other to obtain $\Delta\rho(r)$.

Figure 8 shows $\Delta\rho(r)$ in a slice extending along the axis defined by the center of the unit cell and the Bi adatom as shown in the unit cell graphic at the right of the figure. The blue color is indicative of negative charge density difference and shows electron depletion, whereas the red color refers to an increase in charge density. For Bi, the charge density in the core region (primarily 5d character) increases by 0.07 e/Å^3. Outside the core, the charge density on the Bi 6s does not change much, whereas 6p is somewhat depleted by −0.07 e/Å^3. From a comparison of the size of the core and 6p, it is clear that the total electron density on the Bi adatom decreases upon adsorption. For the Au atoms at the surface, the charge density is also rearranged.

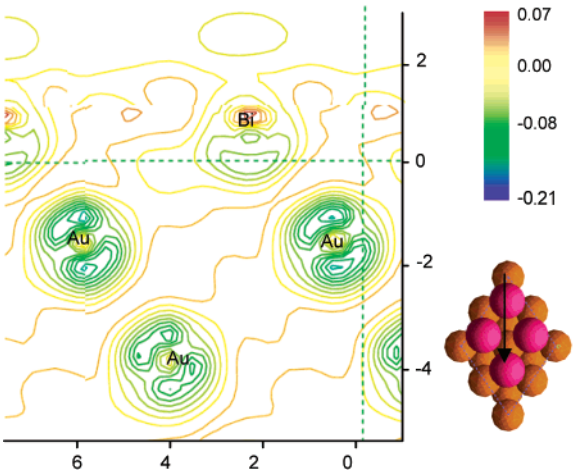

Figure 9. Charge density difference plot for a full monolayer Bi adatoms on Au(111) surface. The plane of the plot contains the arrow shown in the lower right corner of the figure and is normal to the Au surface. Bi adatoms are represented as pink spheres. The unit of charge density is e/Å^3. The unit of both axis is Å.

In the core region, the charge density does not change much. Outside the core region, especially for the Au atom in this slice directly contacting the Bi adatom, electrons in the 5d orbital are strongly depleted and the d_{z^2}-like orbital is reoriented toward the Bi atom. By examining changes in the atomic density of states, it is understood that electrons accumulate near the surface in a level that contains substantial Au 6s character and forms an extra layer of charge.

This analysis indicates that there is substantial charge sharing between the Bi adatom and the Au surface. The Bi donates charge to the Au(111) surface. This charge donation is reflected in the net +0.80 e retained on the Bi adatom and the −0.30 e on Au atoms placed just under it as described in Table 4. The dominant feature of Bi chemisorption on Au(111) surface is depletion of the 6p level on Bi and of the 5d level on Au, with consequent population of the Au 6s level between the two atoms.

3.3.3. Calculation for Bi on Au(111) (50 and 100% Coverages). To evaluate the special properties of the (2 × 2) Bi/Au(111) system, we performed calculations on two other Bi/Au configurations. The 50% coverage system features two Bi adatoms per unit cell, with both on fcc sites. This coverage is close to the experimentally observed ($p \times \sqrt{3}$) structure, which features 63−65% Bi coverage.[7] We also performed calculations on a putative (1 × 1) (100%) structure, where four Bi adatoms were placed on all of the fcc sites on the Au(111) surface. A model of this structure is shown in Figure 9.

Table 5 compares energy, charge, and structural differences arising from the different Bi coverages. As expected, the adsorption energy per adatom decreases with increasing coverage.[61] The 25% coverage system features the highest adsorption energy per Bi adatom, −4.544 eV, which is 0.277 eV more stabilized than the 50% Bi surface and 0.639 eV more stabilized than the 100% structure. As the Bi coverage increases, the distance between the Bi adatom and the closest Au atom increases from 2.68 to 2.94 Å. Alternatively, the calculated Mulliken charge population of the Bi adatoms decreases from +0.81 to +0.19 e, whereas the corresponding charge population

(61) Rojas, M. I.; Del Popolo, M. G.; Leiva, E. P. M. *Langmuir* **2000**, *16*, 9539−9546.

Table 5. Comparison of Results for Different Bi Coverages on Au(111)

Φ_{Bi}	0%	25%	50%	100%
$-E_{ad}$[a] (eV)		4.544	8.516	15.621
$-E_{ad}$/Bi[b] (eV)		4.544	4.258	3.905
$\Delta z_{(Bi-Au1)}$[c] (Å)		2.10	2.14	2.43
q_{Au}[d] (e)	−0.06	−0.30	−0.23	−0.12
q_{Bi}[d] (e)		0.81	0.45	0.19
d(Au−Bi)[e] (Å)		2.6767	2.7305	2.9396

[a] Adsorption energy E_{ad}, calculated as the difference between E_{AuBi} (the total energy for Bi adsorbed on Au) and the sum of E_{Bi} (the free Bi atom energy) and $E_{Au(111)}$ [the isolated Au(111) slab energy]. [b] Adsorption energy E_{ad}, calculated per Bi adatom. [c] Vertical distance between Bi atom and the Au surface. [d] Calculated Mulliken charge population of the Bi atom or the Au atom that is closest to the Bi atom. [e] Distance between the Bi atom and the nearest Au atom.

for the Au atom nearest the Bi decreases from −0.30 to −0.12 e as Bi coverage is increased. These trends suggest that as more Bi atoms are adsorbed on the surface, the interaction between Bi adatoms and the Au(111) surface decreases.

Figure 9 shows the total charge density difference, $\Delta\rho(r)$, from the 100% Bi structure on Au(111) surface in a slice indicated by an arrow on the unit cell structure shown in the right corner of the figure. The charge density in the core region of the Bi adatom increases by +0.07 e/Å^3, whereas there are slight decreases in the Bi 6p level outside the core. For Au surface atoms, the charge density in the core region does not change much. Charge depletion occurs in the 5d orbital, which is reoriented toward the Bi adatoms on surface.

There are two points of comparison between the 100 and 25% Bi coverage systems. First, the 25% Bi system features charge accumulation between the adatom and the surface, a feature not found in the 100% system. Second, the degree of charge depletion from the surface atoms is a factor of ∼2 greater in the 25% system relative to that in the 100% system. This comparison indicates that the 100% system is more metallic and the 25% system more covalent relative to each other.

3.3.4. Calculation for H_2O_2 on Bi/Au(111) Surface. As the next step in evaluating the reactivity of H_2O_2 on the Bi-modified Au(111) surface, we added H_2O_2 to the Bi/Au(111) slab described above. Although there has been considerable activity modeling the adsorption of O_2 on metal surfaces, especially those described by Pt clusters,[62] there has been less activity examining the interaction of metals with peroxide. In this section, we examine the way in which H_2O_2 interacts with the bare Au and the 25, 50, and 100% Bi-modified surfaces.

3.3.4.1. Calculation for H_2O_2 on the Bi/Au(111) Surface with Different Bi Coverages. Figure 10, pieces a, b, c, and d, shows the energy-minimized structures adopted by H_2O_2 on the bare Au(111) surface and the 25, 50, and 100% Bi-modified Au(111) surface, respectively. In these calculations, the positions of the Au and Bi atoms are fixed, whereas the atoms in the peroxide are allowed to vary. The energy-minimized structures adopted by peroxide are independent of starting geometry. In the case of 25% Bi/Au(111), a two unit cell picture is shown for a clear evaluation of the interaction between H_2O_2 and the Bi atoms. A free H_2O_2 molecule is shown in Figure 10e for comparison.

Calculation of the structure of the free peroxide produced calculated O−O and O−H bond lengths of 1.462 and 0.978 Å,

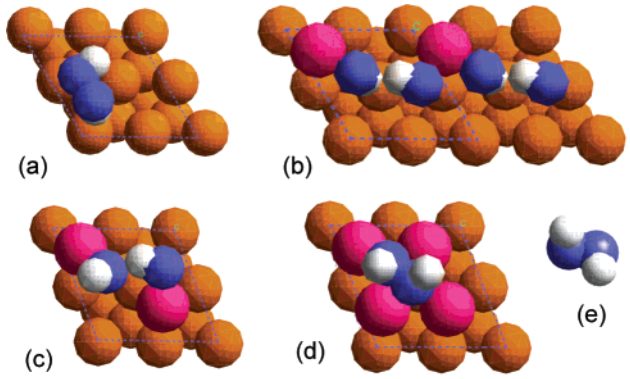

Figure 10. Illustration of the geometry of H_2O_2 adsorption on Bi/Au(111): (a, b, c, d) 0, 25, 50, and 100% Bi on Au(111) cases, respectively. Two unit cells are shown in (b) for a clear picture of H_2O_2 interaction with two Bi atoms. A free H_2O_2 molecule is shown in (e) for comparison. Au, Bi, O, and H atoms are orange, pink, blue, and white balls, respectively.

respectively, which are close to the experimental values of 1.47 and 0.97 Å.[63] The calculated O−O−H angle and the dihedral H−O−O−H angle are 100.4 and 115.0°, respectively. This also agrees with the experimental values of 100 and 120°.

On the bare Au(111) surface, H_2O_2 was calculated to adsorb with the two O atoms on two bridge sites, and the molecule centered above a fcc site. On the 25% coverage Bi/Au(111) surface, one O is found above the hcp site with the other above a bridge site. Both O atoms are found close to the Bi adatoms. On the 50% Bi/Au(111) surface, the two O atoms are found close to a Bi atom above an hcp site. As the surface coverage increases to 100%, H_2O_2 adsorbs on the hcp site, with one O atom above the fcc site and the other one near a bridge site.

The geometry and energy comparison of H_2O_2 adsorption on Bi/Au(111) surfaces are given in Table 6. By comparing the adsorption energy change on the different surfaces, it is clear that H_2O_2 adsorption on 25% Bi/Au(111) is strongest, being some 3.152 eV more stabilized than on bare Au(111), 0.146 eV more stabilized than on 50% Bi/Au(111), and 0.967 eV more stabilized than on the 100% Bi structure.

The Mulliken charge populations of all the Au, Bi, and O atoms were also calculated and are shown in Table 6. For all surfaces, the change of charge on the Au atoms is <0.1 e upon H_2O_2 adsorption. This implies that Au atoms interact with H_2O_2 only weakly. In addition, on both the bare Au surface and the 100% Bi structure, the O atoms of H_2O_2 are calculated with a charge of −0.48 e, which is some 0.09 e more positive than that exhibited by the O atom in free H_2O_2.

When Bi is present and peroxide is adsorbed, the calculated charge change on these species changes considerably as the Bi coverage changes. On the 25% Bi/Au(111) surface, the O atoms attain 0.29 and 0.27 e more negative charge relative to free H_2O_2. Correspondingly, the Bi adatom becomes 0.95 e more positive. These changes suggest that there is a strong interaction between the peroxide and Bi. Similarly, on the 50% Bi/Au(111) surface, the Bi atoms become 1.06 and 0.33 e more positive, whereas the O atoms become 0.30 and 0.29 e more negative. Clearly, Bi and O atoms interact with each other strongly on this surface, too.

A clearer picture of the interaction between Bi and H_2O_2 is obtained by examining the calculated O−O bond lengths in these

(62) Sidik, R. A.; Anderson, A. B. *J. Electroanal. Chem.* **2002**, *528*, 69−76.

(63) Giguere, P. A. *J. Chem. Educ.* **1983**, *60*, 399−401.

Table 6. Comparison of Results for H_2O_2 Adsorption on Bi/Au(111) with Different Bi Coverages and with H_2O_2 End-on to the 25% Bi/Au(111) System

Φ_{Bi}	0%	25%	50%	100%	end-on
$-E_{ads}$[a] (eV)	0.076	3.228	3.082	2.271	−0.908
$-\Delta E_{ads}$[b] (eV)	0	3.152	3.006	2.195	0.984
d(O−O)[c] (Å)	1.4589	2.9655	2.6901	1.4604	1.477
d(Bi−O) (Å)		2.025/2.055	2.117/2.171	3.839/4.580	2.321
$\Delta z_{(Au-O)}$[d] (Å)		3.15/3.53	3.63/3.83	5.60	
Δq_{Au}[e] (e)	−0.07	0.06	0.05	−0.08	0.00
q_{Bi} (e)		1.76	1.50/0.77	0.43/0.39	0.99
Δq_{Bi}[f] (e)		0.95	1.06/0.33	0.24/0.20	0.18
q_O (e)	−0.51/−0.48	−0.86/−0.84	−0.88/−0.87	−0.48/−0.48	−0.55/−0.47
Δq_O[g] (e)	0.06/0.09	−0.29/−0.27	−0.31/−0.30	0.09/0.09	0.02/0.10

[a] Adsorption energy E_{ad}, calculated as the difference between the H_2O_2 adsorption on the slab energy (E_{total}) and the sum of the free H_2O_2 molecule energy ($E_{H_2O_2}$) and the Bi/Au(111) slab energy (E_{slab}). [b] Change of adsorption energy of peroxide due to the presence of Bi adatoms, $\Delta E_{ads} = E_{ads}$ (n% Bi) $- E_{ads}$ (0% Bi). [c] O−O bond length in free H_2O_2 is 1.462 Å. [d] Vertical distance between the lower O atom and the Au surface. [e] Mulliken charge population difference on the Au atom closest to Bi: $q_{H_2O_2/Bi/Au(111)} - q_{Bi/Au(111)}$. [f] Mulliken charge population difference on the Bi atom: $q_{H_2O_2/Bi/Au(111)} - q_{Bi/Au(111)}$. [g] Mulliken charge population difference on the O atom: $q_{H_2O_2/Bi/Au(111)} - q_{H_2O_2}$.

systems. On both bare Au and the 100% Bi system, the O−O bond length changes only slightly to 1.460 and 1.459 Å, respectively. Likewise, the Bi−O distances are calculated to be 3.84 and 4.58 Å in the 100% coverage system, and the Au−O distances are calculated to be 3.11 and 3.75 Å in the bare Au case. These distances are well outside the range of any significant interaction between O and either Bi or Au.

However, on the 25% Bi surface, the O−O bond of H_2O_2 stretches from 1.462 to 2.966 Å. In gas phase reactivity studies, peroxide is considered to be dissociated when the O−O bond length reaches ∼3 Å, and calculations indicate the presence of a transition state around this value.[64] Alternatively, the calculated distance between Bi and O atoms is only 2.025 and 2.055 Å, which is within the range of a Bi−O bond.[65] In the 50% Bi system, the calculated O−O bond length has also increased to 2.69 Å, a value which is not as large as that found in the 25% coverage system. The corresponding Bi−O distances in the 50% system are 2.117 and 2.171 Å, bond lengths that are greater than that found with the 25% coverage system.

3.3.4.2. Interaction of H_2O_2 with (2 × 2) Bi /Au(111). 3.3.4.2.1. Density of States. To further clarify the interaction between H_2O_2 and Bi, the density of states for Au, 25% Bi/Au(111), free peroxide, and H_2O_2/Bi/Au(111), are calculated and shown in Figure 11. The Fermi level in the metallic systems is indicated by the arrow.

In Figure 11a the bare Au(111) system, the Fermi level is at −6.776 eV. Shown in the figure is only the region from −10 to +4.0 eV. The DOS calculated agrees qualitatively with that published previously.[37] In the 25% Bi/Au(111) system (Figure 11b), the Fermi level moves to −8.026 eV. The negative shift of the Fermi level is caused by interaction of the Au surface with low-lying states of the Bi adatom. The lowest state shown is state ii at −11.49 eV, which originates primarily from the 6s orbital on the Bi adatom. A small contribution to state ii also comes from the s and p orbitals of those Au atoms that contact directly with Bi adatom. The region between −10 and 0 eV contains contributions from the 6d orbitals of Au atoms and the 6p orbital of Bi. For states above 0 eV, state iv at 1.28 eV comes from the lower shift of the 6p orbital of free Bi atom, at 4.06 and 5.00 eV, and state 4 of the Au(111) system at 1.30 eV.

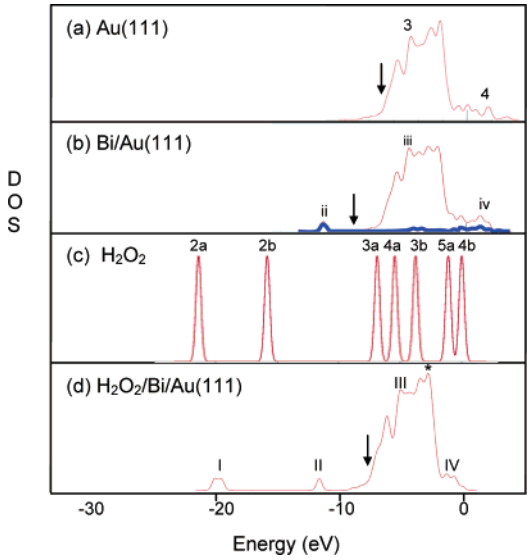

Figure 11. Density of states comparison for Au(111), 25% Bi/Au(111), free H_2O_2, and H_2O_2 adsorption on 25% Bi/Au(111) surface. Arrows indicate the Fermi level. The blue line in (b) is the contribution from Bi to the density of states in the 25% Bi/Au system.

The density of states from the free H_2O_2 molecule are calculated and shown in Figure 11c. The calculation shows five occupied states in the high-energy region and two levels at lower energies. The lowest two levels, 2a at −21.41 eV and 2b at −15.824 eV, derive primarily from the 2s orbital of the O atoms. The 3a level at −6.88 eV arises from the p orbitals directed along the O−O bond. The 4a, 3b, 5a, and 4b levels all derive from combinations of the p orbitals orthogonal to the O−O axis, along with contributions from the H s orbitals.[66]

Experimentally, the first ionization from free peroxide occurs at −11.69 eV, >10 eV more negative than that calculated here. In the CASTEP program, the zero of energy for molecules is defined as the level of highest occupation and is not referenced to vacuum. However, the difference in energy between different orbitals is in accord with the experimentally measured vertical ionization energies.[67] Exact correspondence between the experiment and the calculation would require a calculation of the ionization potentials for peroxide, which was not attempted.

When the peroxide interacts with the 25% Bi/Au(111) surface, the Fermi level shifts to −7.308 eV, which is ∼0.7 eV more

(64) Akiya, N.; Savage, P. E. *J. Phys. Chem. A* **2000**, *104*, 4441−4448.
(65) Betsch, R. J.; White, W. B. *Spectrochim. Acta, Part A* **1978**, *34A*, 505−514.
(66) Epiotis, N. D.; Larson, J. R.; Eaton, H. H. *Croat. Chem. Acta* **1985**, *57*, 1031−1053.
(67) Takeshita, K.; Mukherjee, P. K. *Chem. Phys. Lett.* **1989**, *160*, 193−199.

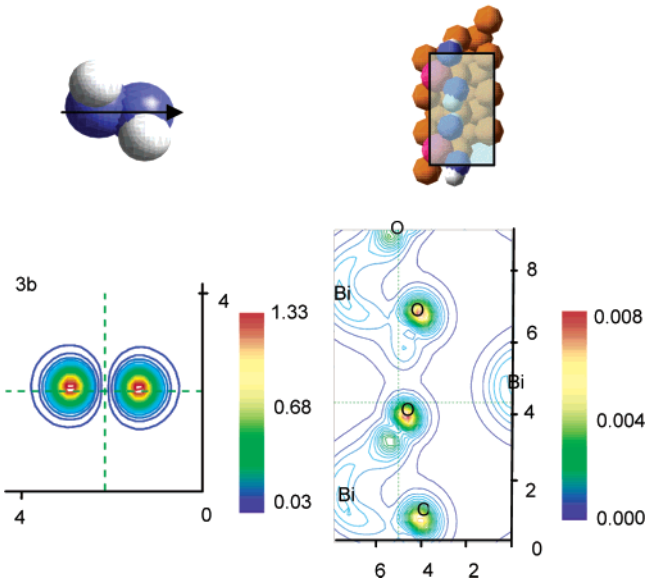

Figure 12. Charge density for the 3b orbital of free H_2O_2 (left), compared with the corresponding orbitals at $E = -4.2$ eV following H_2O_2 adsorption on Bi(2×2) Au(111) (right). The plane of the plot, shown schematically at the top of the figure, is parallel to the surface and contains the center of both O atoms. The dimension for each plot is given in Å. The unit of charge density is e/Å^3.

positive than the Bi/Au(111) system without H_2O_2. This positive shift of the Fermi level is associated with increased electron density on the surface due to charge transfer between the peroxide and the Bi/Au(111) structure. Additionally, features associated with the free peroxide molecule are strongly perturbed, as shown in Figure 11d. A new DOS feature I grows in place of distinct 2a and 2b levels as the O−O bond in the peroxide is cleaved and the Bi−OH species is formed. Feature I is composed of two levels at −20.05 and −19.47 eV, which originate from a combination of both the 2a and 2b levels of the free H_2O_2 molecule. Calculation of atomic density states shows that the Bi atom also contributes to these peaks. Peak II at −11.58 eV derives mainly from the interaction of the Bi 6s levels (formerly peak ii in Figure 12b) and the 3a and 4a levels of H_2O_2. Nearly 70% of the peak density is from the Bi atom, whereas H_2O_2 donates the rest. In the region above −10 eV, there are additional contributions from O, Bi, and (primarily) Au. Upon H_2O_2 adsorption, the states from the 6p orbital of the Bi adatom shift −4 eV to interact with levels originally in the 3b, 5a, and 4b of H_2O_2. There is relatively little perturbation of Au levels upon the introduction of peroxide. This analysis suggests a strong interaction between Bi and O from peroxide.

3.3.4.2.2. Charge Density of Orbitals. Figure 12 shows the charge density for free peroxide and the adsorption system calculated at an energy of −4.2 eV, which is where the DOS indicates the presence of a strong Bi−O interaction. The left column shows the orbital contours for peroxide along the O−O bond, showing the 3b interactions. The right column shows the corresponding level after interaction with the Bi/Au(111)(25%) system. The figure shows that there is relatively little electron density between the O atoms that formerly made up peroxide and substantial electron density between O and Bi. This shows that the O−O bond in peroxide is cleaved and replaced with two Bi−OH bonds.

3.3.5. Calculation for H_2O_2 Adsorption End-on Bi/Au(111) Surface. End-on adsorption of peroxide to the active surface is another possible way in which reduction of this species could be accomplished.[2] To test this geometry for our system, we performed total energy calculations for H_2O_2 adsorbed end-on to the (2×2) Bi surface. Energy minimization of the end-on geometry always results in the Bi−OH geometry discussed above. This implies that the end-on geometry is not stable relative to cleaved peroxide on 25% Bi/Au(111).

To further examine the end-on adsorption of peroxide, we fixed the position of all the atoms. We examined peroxide adsorbed end-on in several different positions, including above the Bi, above the Au, and between the Au and Bi. The lowest energy was obtained with H_2O_2 adsorbed atop the Bi adatom. Table 6 compares parameters for this interaction with those for the optimized system discussed above.

The end-on adsorption of H_2O_2 has a positive adsorption energy, 0.908 eV, which implies that this geometry is not stable. Alternatively, the charge on Bi atoms increases only 0.19 e, whereas the O atoms gain positive charges of 0.02 and 0.10 e. H_2O_2 adsorbed end-on on the 25% Bi/Au(111) surface is not energetically favored.

4. Discussion

4.1. SERS Measurements. The measurements and calculations reported above provide considerable insight into the mechanism of peroxide electroreduction on the Bi upd-modified Au(111) surface. In particular, the SERS measurements strongly support a role for the Bi−OH species as an intermediate in the electroreduction processes, along with other possible Bi−O species.

One of the most problematic features of SERS studies is that they are performed not on single-crystal surfaces but rather surfaces that have been roughened. The exact site of the SERS response on the electrode surface is still unclear and may vary from measurement to measurement.[68] These aspects of SERS complicate assignment of spectroscopic features to structural effects. In this work, we show that the electrochemical response from the SERS-active electrode and the Bi-modified Au(111) surface—well characterized using AFM, STM, and surface X-ray scattering—are quite similar to each other. Both surfaces exhibit voltammetric features due to Bi upd, with the potential shift between the two understandable in terms of work function differences between the two surfaces. Both surfaces also exhibit an electrocatalytic response that features the characteristic off−on−off pattern. On the Au(111) surface, the potential region of catalytic activity is associated with the (2×2) Bi structure. The similarity of the RDE measurements between the two surfaces suggests that there is some substantial similarity between the single-crystal and polycrystalline systems.

SERS measurements show the presence of a substantial signal attributable to peroxide in systems absent Bi but containing peroxide. Likewise, when Bi is present, but not peroxide, there is a signal attributed to Bi−OH (band 6), but only at very positive potentials ($E > +0.7$ V). On single-crystal surfaces, Bi is desorbed by these potentials and the polycrystalline voltammetry reported here likewise gives a similar indication. In a solution containing only perchloric acid, a Au−$OH_{ads}^{\gamma-}$ bending vibration (band 2) was observed with approximately the same potential dependence as band 6. Interestingly, the Au−OH stretch was not observed in measurements where Bi is

(68) Garrell, R. L. *Anal. Chem.* **1989**, *61*, 401A−402A.

present. After the addition of Bi^{3+}, band 2 was no longer observed, which may reflect the higher affinity of Bi for hydroxide relative to Au. The Bi−OH signal may then be attributable to Bi entrained in the rough Au surface or to soluble Bi species, which are close to the surface. In any event, the potential dependence of this band suggests that it is associated with events surrounding Au electrode oxidation and not peroxide reduction.

When both Bi and peroxide are present, there are two signals associated with Bi−oxygen species. Both of these signals exhibit a potential dependence such that they are maximized at potentials just positive of the region of maximum catalytic response. As the potential is swept to more negative values, and current associated with peroxide reduction begins to flow, these signals both decay rapidly. It is thus reasonable to associate these signals with species present on the surface arising from both Bi and peroxide, which are not actually present during the flow of electrons describing the reduction process.

The band at 972 cm^{-1} is associated with a Bi−OH species, while that at 625 cm^{-1} is associated with a Bi_2O_2 tetramer. It is reasonable to associate the O source that gives rise to these species with peroxide, because neither band is present at lower potentials in the absence of this species. The SERS results suggest that these Bi−O species are intermediates in the electroreduction process and are consequences of the interaction of peroxide with the Bi-modified surface without the passage of current associated with the formal reduction of the peroxide.

Previous chronocoulometric work from this group suggested that an OH species is coadsorbed with Bi in the (2 × 2) structure with a Bi/OH ratio somewhere between 1:1 and 1:2.[7] In the absence of peroxide, there is no band attributable to Bi−OH or Au−OH (the stretching mode for Au−OH is expected in the range between 580 and 425 cm^{-1}, whereas the bending mode is at ∼790 cm^{-1}) in the potential region where Bi is upd deposited on the Au surface. This suggests that any OH present in this system absent peroxide is weakly interacting with the Bi/Au(111) system.

4.2. Calculations. To clarify ideas about the interaction of peroxide and Bi on the Au surface, we performed detailed calculations examining the interaction of Bi, peroxide, and Au as they relate to the electroreduction process. Because the calculations do not formally allow for the addition of two electrons with the presence of two protons to model the electroreduction event, we are not able to model the process completely. However, both the calculation and the experiment agree on the importance of the $Bi(OH)_2$ species as an intermediate in the electroreduction event. In what follows, we first examine the description of the surface following modification with Bi. We next show how this surface structure changes following exposure to peroxide.

4.2.1. Bi Upd on Au without Peroxide. A formal description of the upd process would involve reduction of the Bi^{3+} species initially present in solution. The present calculation starts with fully discharged Bi and then associates this atom with the Au surface. The use of Bi^0 in this calculation is the same as formally requiring Bi to be fully discharged during upd. Chronocoulometric measurements support this description of the Bi state, because a requirement for a full three electrons per Bi was found throughout the Bi upd potential region.[7] Thus, the initial condition of a fully discharged Bi is thought to be reasonable. We next study possible charges remaining on the Au surface during the formation of the (2 × 2) Bi adlayer. The potential of zero charge (pzc) for Au(111) in perchloric acid solution is 0.48 V. The Bi (2 × 2) adlayer begins to form on Au(111) in the potential region around ∼0.45 V. This suggests that an uncharged surface is a good approximation of the state of electrode.

Our calculations show that Bi and Au interact strongly. With 25% coverage, the bond between Au and Bi is found to exhibit considerable covalent character, with 6s-type electron density found between Bi and the nearest-neighbor Au atoms. As the coverage of Bi is increased, the interaction becomes weaker on a per atom basis, a conclusion also suggested on the basis of calculations employing embedded atom model (EAM) potentials.[61] In addition, increasing the Bi coverage involves charge accumulation preferentially in the internuclear region rather than between the Bi atom and the near Au atoms. This internuclear region accumulation suggests that the bond between Bi and Au atoms becomes more metallic.[69,70]

The calculations also show that there are changes in the nature of the Au surface upon association with Bi at 25% coverage. The calculated Mulliken charge on Au atoms directly under the Bi adatom increases from −0.06 e without Bi to −0.30 e upon Bi adsorption. Interestingly, the central Au atom in the (2 × 2) unit cell (Figure 6, top view**)** is much more positive than the other surface Au atoms. We previously associated this Au atom as the site of SCN^- adsorption during poisoning experiments.[39] The charge on the other Au atoms (second and third layers) in the calculation does not change substantially.

Upd has been the subject of several previous calculation efforts. In the work of Leiva, EAM potentials were used to evaluate contributions to the binding energy between the upd adatom and the surface.[25,71] The adsorption energy per monolayer of adatom ranges from −2.8 to −3.5 eV within the range of noble metals they studied.[22] In our system, the adsorption energy per Bi atom in a monolayer is −3.89 eV because of the strong interaction between Bi and the Au substrate.

4.2.2. Peroxide Reduction on Bi Upd on Au. On the basis of the calculation and experimental results, a mechanism for the electroreduction of H_2O_2 on the (2 × 2) Bi/Au(111) surface is proposed in Figure 13. The initial reactants are the (2 × 2) Bi/Au(111) surface and free H_2O_2. In the first step, H_2O_2 is chemisorbed on the surface by two Bi centers forming two Bi-$(OH)_2$ moieties. The O−O bond is cleaved, and Bi−O bonds are formed. The calculation suggests that the distance between the Bi adatoms, which is just large enough so that two Bi can interact with the incoming peroxide, aids cleavage of the O−O bond. The initial energy of the O−O bond in H_2O_2 is 1.517 eV.[2] The energy of a Bi−O bond formed on the surface is 2.373 eV, giving a total stabilization with the formation of two Bi−O bonds of −3.228 eV. The charge on the Bi goes from +0.81 e before peroxide interaction to +1.76 e afterward, indicating that the Bi is oxidized. The SERS results suggest that the tetracycle Bi_2O_2 (in brackets in Figure 13) forms as an intermediate during this step. Unfortunately, calculation of this complex requires use of a larger unit cell than was considered in these calculations.

(69) Mayer, M.; Pacchioni, G.; Rosch, N. *Surf. Sci.* **1998**, *412*, 616−624.
(70) Doll, K. *Eur. Phys. J. B: Condensed Matter Phys.* **2001**, *22*, 389−393.
(71) Leiva, E. P. M.; Del Popolo, M. G.; Schmickler, W. *Chem. Phys. Lett.* **2000**, *320*, 393−397.

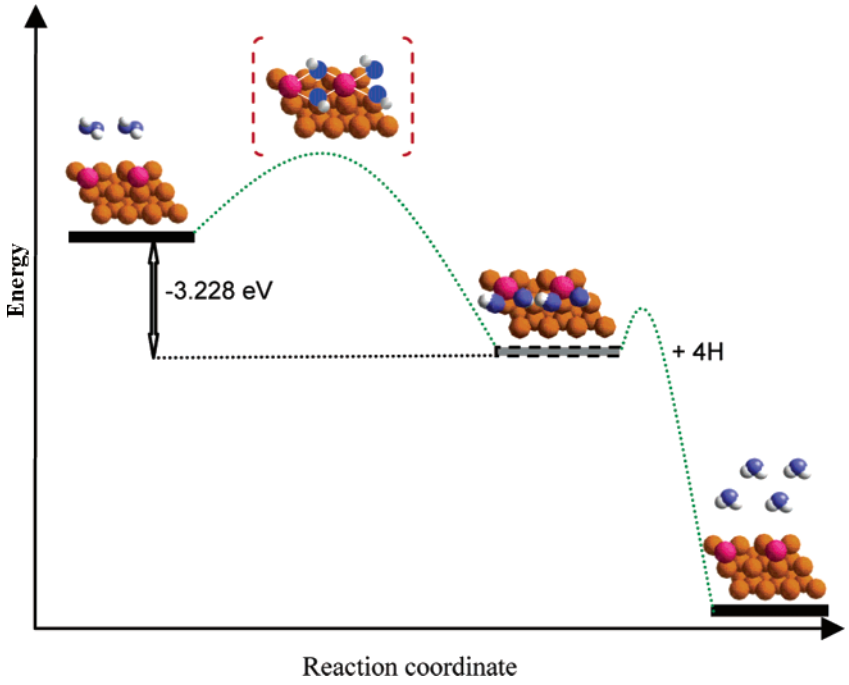

Figure 13. Proposed hydrogen peroxide reduction mechanism on the (2 × 2) Bi/Au(111) surface. The structure enclosed in red brackets is an intermediate not calculated in this work. The orange, pink, blue, and white balls represent Au, Bi, O, and H atoms, respectively.

The next step in the electroreduction process is reduction of the Bi−OH complex, leading to cleavage of the Bi−O bond. The density of state calculation shows that there is a low-lying, unoccupied state at ∼ −2.6 eV (marked with a star in Figure 11) that is predominately antibonding between O and Bi. It is reasonable to expect that the reducing electron will populate this state. The Bi center is then formally reduced, and the resultant OH^- reacts with H^+ in solution to yield H_2O. The Pourbaix diagram for Bi [72] shows the presence of a Bi−OH species at low pH values that is reduced to Bi around 0.2 V, near the experimental potential of peroxide reduction on the Bi (2 × 2) surface. We note that the Bi−OH species in the Pourbaix diagram is found between pH 2 and 3 and our measurements are carried out at pH 1. However, because the peroxide reduction reaction consumes protons, it is reasonable to expect that the effective pH at the electrode surface will be somewhat higher than the bulk solution value.

4.2.3. Peroxide Association on Surfaces with Higher Bi Coverage. As the potential is swept to more negative values, the (2 × 2) Bi adlattice is transformed to the ($p \times \sqrt{3}$) structure and peroxide electroreduction activity ceases. The SERS shows that neither the $Bi(OH)_2$ or Bi_2O_2 species observed at more positive potentials are present in this potential region. The calculations suggest that the O atoms of H_2O_2 interact strongly with two Bi adatoms when Bi is on the surface. As the distance between Bi adatoms decreases with increasing coverage, the O−O bond of the H_2O_2 can accommodate the interaction with Bi without breaking. The O−O bond of peroxide is thought be cleaved when it approaches a length of ∼3.0 Å. However, the calculated O−O distance is only 2.69 Å on the 50% Bi/Au(111) surface and 1.46 Å (the same as free H_2O_2) on the 100% Bi/Au(111) surface. The Bi coverage in the ($p \times \sqrt{3}$) structure is ∼63% with a Bi−Bi distance of ∼3.4 Å, quite a bit less than the 5.76 Å Bi−Bi distance in the (2 × 2) structure. These calculations show that in addition to strong association of peroxide with the Bi surface, a second requirement for O−O bond cleavage is the presence of the pocket formed by the (2 × 2) structure, the dimensions of which help to effect bond cleavage.

5. Conclusions

Both calculation and experiment strongly support the formation of a $Bi(OH)_2$ intermediate in the electroreduction of peroxide to water on the (2 × 2) Bi-modified Au(111) surface. The intermediate forms as a consequence of increased stability afforded by two Bi−OH bonds relative to the O−O bond in H_2O_2. Cleavage of the O−O bond arises as a consequence of the distance between adjacent Bi adatoms on the Au(111) surface. When this distance becomes too small, the O−O bond is not cleaved, and peroxide remains on the surface. The upd structure that is responsible for catalytic activity exhibits more covalent character than the more metallic higher coverages, which are not catalytically active. The reduction of the Bi−OH complex yields OH^- that combines with H^+ in solution to form water.

Bound hydroxide is also implicated in the electroreduction of peroxide and dioxygen on other materials, such as Pt and Ag in acid, and this study confirms the ubiquity of this species in peroxide and dioxygen reduction. Although the specific role of the hydroxide may vary from surface to surface, formation of a M−OH species would seem to be one criterion for peroxide electroreduction activity. The present study shows that tuning the distance between metal centers that bind hydroxide is one way to cleave the O−O bond of the peroxide.

These results suggest that new catalysts exhibiting facile electroreduction behavior toward dioxygen or peroxide can likely be affected in systems which exhibit two features. First, the metal centers in these materials will spontaneously decom-

(72) Pourbaix, M. *Atlas of Electrochemical Equilibria in Aqueous Solutions*; National Association of Corrosion Engineers: Houston, TX, 1974.

pose peroxide to yield M−OH moieties. Second, these M−OH moieties will be easily reduced. We are in the process of synthesizing complexes exhibiting these features.

Acknowledgment. X.L. thanks the Department of Chemistry for financial support in the form of a Carl Shipp Marvel fellowship. This work was partially supported by National Computational Science Alliance under CHE030003 and utilized the NCSA Origin2000. We thank R. Strange and J. O. White of the Laser Laboratory in the Frederick Seitz Materials Research Laboratory at the University of Illinois for their assistance in Raman data acquisition. The Laser Laboratory is funded by Department of Energy Grant DE-FG02-96ER45439 through the Materials Research Laboratory at the University of Illinois. This work was funded by the NSF (CHE-02-37683), which is gratefully acknowledged.

Supporting Information Available: Geometries (Cartesian coordinates) of all calculated slabs. This material is available free of charge via the Internet at http://pubs.acs.org.

JA034125Q